A&A 533, A101 (2011)
DOI: 10.1051/0004-6361/201117318

Astronomy & Astrophysics

VLT observations of the two *Fermi* pulsars PSR J1357−6429 and PSR J1048−5832⋆

R. P. Mignani[1,2], A. Shearer[3], A. De Luca[4,5,6], P. Moran[3], S. Collins[3], and M. Marelli[5,7]

[1] Mullard Space Science Laboratory, University College London, Holmbury St. Mary, Dorking, Surrey, RH5 6NT, UK
e-mail: rm2@mssl.ucl.ac.uk
[2] Institute of Astronomy, University of Zielona Góra, Lubuska 2, 65-265 Zielona Góra, Poland
[3] Centre for Astronomy, National University of Ireland, Newcastle Road, Galway, Ireland
[4] IUSS – Istituto Universitario di Studi Superiori, viale Lungo Ticino Sforza, 56, 27100 Pavia, Italy
[5] INAF – Istituto di Astrofisica Spaziale e Fisica Cosmica Milano, via E. Bassini 15, 20133 Milano, Italy
[6] INFN – Istituto Nazionale di Fisica Nucleare, sezione di Pavia, via A. Bassi 6, 27100 Pavia, Italy
[7] Universitá degli Studi dell' Insubria, via Ravasi 2, 21100 Varese, Italy

Received 23 May 2011 / Accepted 21 July 2011

ABSTRACT

Context. Optical observations of pulsars are crucial to studying the neutron star properties from the structure and composition of the interior to the properties and geometry of the magnetosphere. Historically, X and γ-ray observations have paved the way to pulsar optical identifications. The launch of the *Fermi* Gamma-ray Space Telescope opened new perspectives in the optical-to-γ-ray studies of neutron stars with the detection of more than 80 γ-ray pulsars.

Aims. Here, we aim to search for optical emission from two *Fermi* pulsars that are interesting targets on the basis of their spin-down age, energetics, and distance. PSR J1357−6429 is a Vela-like pulsar (P = 166.1 ms; τ = 7.31 kyr), at a distance of ∼2.4 kpc with a rotational energy loss rate $\dot{E} \sim 3 \times 10^{36}$ erg s^{-1}. PSR J1048−5832 is also a Vela-like (P = 123.6 ms; τ = 20.3 kyr) pulsar at a distance of ∼2.7 kpc and with a $\dot{E} \sim 2 \times 10^{36}$ erg s^{-1}. The two pulsars and their pulsar wind nebulae (PWNe) are also detected in X-rays by *Chandra* and *XMM-Newton*. No deep optical observations of these two pulsars have been reported so far.

Methods. We used multi-band optical images (V, R, I) taken with the Very Large Telescope (VLT) and available in the European Southern Observatory (ESO) archive to search for, or put tight constraints on, their optical emission.

Results. We re-assessed the positions of the two pulsars from the analyses of all the available *Chandra* observations and the comparison with the published radio coordinates. For PSR J1357−6429, this yielded a tentative proper motion $\mu = 0\farcs17 \pm 0\farcs055$ yr^{-1} (70° ± 15° position angle). We did not detect any candidate counterparts to PSR J1357−6429 and PSR J1048−5832 down to $V \sim 27$ and ∼27.6, respectively, although for the former we found possible evidence of a faint, unresolved object at the *Chandra* position. Our limits imply an efficiency in converting spin-down power into optical luminosity $\lesssim 7 \times 10^{-7}$ and $\lesssim 6 \times 10^{-6}$, possibly close to that of the Vela pulsar.

Conclusions. Observations with the *Hubble* Space Telescope (HST) are required to identify PSR J1357−6429 against nearby field stars. Owing to the high extinction ($A_V \sim 5$) and the presence of a molecular cloud complex, near-infrared observations of PSR J1048−5832 are better suited to spotting its candidate counterpart.

Key words. stars: neutron – pulsars: individual: PSR J1357–6429 – pulsars: individual: PSR J1048–5832

1. Introduction

Optical observations of rotation-powered pulsars are important for completing the picture of their multi-wavelength phenomenology, and they play a major role in studying the intrinsic properties of neutron stars, from the interior structure and composition to the atmosphere and magnetosphere properties, as well as in understanding their formation and evolution (see, e.g. Mignani 2010a, b).

More than 40 years have gone by since the optical identification of the Crab pulsar. Since then, only ten pulsars have been firmly identified in the optical (Mignani 2009a, 2011), mostly with the *Hubble* Space Telescope (HST) and the telescopes of the European Southern Observatory (ESO), like the Very Large Telescope (VLT), which have played a fundamental role in pulsar optical astronomy (Mignani 2010c, 2009b). Together with those in the radio band, high-energy observations play a pivotal role in paving the way to the optical identification of pulsars. In particular, five out of the seven γ-ray pulsars detected by NASA's *Compton Gamma-ray Observatory* (CGRO) satellite (see, e.g. Thompson 2008) have also been detected in the optical, suggesting that γ-ray detections indicate promising candidates for optical observations, since the emission at both energies seems to correlate with the strength of the magnetic field at the light cylinder (Shearer & Golden 2001; Shearer et al. 2010).

The launch of NASA's *Fermi* Gamma-ray Space Telescope in June 2008 represents a revolution in γ-ray observations of pulsars. The Large Area Telescope (LAT; Atwood et al. 2009) has detected more than 80 γ-ray pulsars (Abdo et al. 2011). While systematic observations of *Fermi* pulsars are performed in the X-rays (e.g., Marelli et al. 2011), for most of them no deep optical observations have been carried out so far (Mignani et al., in prep.). An exploratory survey in the northern hemisphere has

⋆ Based on observations made with the European Southern Observatory telescopes obtained from the ESO/ST-ECF Science Archive Facility.

been carried out with 2.5 m/4 m-class telescopes at the La Palma Observatory, but no pulsar has been detected down to $V \approx 23$–26 (Shearer et al., in prep.), while in the southern hemisphere a dedicated survey with the VLT is in progress (Mignani et al. 2011). In addition, VLT observations of three *Fermi* pulsars, PSR J1357−6429, PSR J1048−5832, and the ms binary pulsar PSR J0613−0200 (Abdo et al. 2010) are available in the public ESO archive. Unfortunately, for the last one an incorrect windowing of the detector cut the pulsar position out of the field-of-view.

PSR J1357−6429 is a young ($\tau \sim 7.3$ kyr), Vela-like pulsar discovered in radio (Camilo et al. 2004) during the 1347 MHz Parkes multi-beam survey of the Galactic plane. Its period ($P = 166.1$ ms) and period derivative ($\dot{P} = 3.60 \times 10^{-13}$ s s^{-1}) yield a rotational energy loss rate $\dot{E} \sim 3.1 \times 10^{36}$ erg s^{-1} and a magnetic field $B = 7.83 \times 10^{12}$ G. The pulsar dispersion measure (DM = 127.2 ± 0.5 cm^{-3} pc; Camilo et al. 2004) yields a distance of 2.4 ± 0.6 kpc, according to the NE2001 Galactic electron density models of Cordes & Lazio (2002). X-ray emission at 2–10 keV from PSR J1357−6429 has been discovered by our group (Esposito et al. 2007) from *Chandra* and *XMM-Newton* observations. The pulsar X-ray emission appeared point-like, with no obvious evidence of a pulsar wind nebula (PWN). No pulsations were detected down to a 3σ upper limit of 30% on the pulsed fraction (2–10 keV). However, based on the same *Chandra* and *XMM-Newton* data sets Zavlin (2007) claimed to find evidence of a compact PWN and of X-ray pulsations, both of which are now confirmed by new *Chandra* and *XMM-Newton* observations (Lemoine-Goumard et al. 2011; Chang et al. 2011).

PSR J1357−6429 has possibly been detected as a γ-ray pulsar at ≳100 MeV by the Astrorivelatore Gamma ad Immagini LEggero (AGILE) with a detection significance of 4.7σ (Pellizzoni et al. 2009). Recently, ithas also been detected by *Fermi* (Lemoine-Goumard et al. 2011), while its associated PWN has been detected at TeV energies by HESS (Abramowski et al. 2011). PSR J1048−5832 is also a young (20.3 kyr), Vela-like radio pulsar, which was discovered during a 1420 MHz radio survey of the Galactic plane (Johnston et al. 1992). The pulsar period ($P = 123.6$ ms) and period derivative ($\dot{P} = 9.63 \times 10^{-14}$ s s^{-1}) yield a rotational energy-loss rate $\dot{E} \sim 2 \times 10^{36}$ erg s^{-1} and a magnetic field $B = 3.49 \times 10^{12}$ G. The DM (129 ± 0.1 cm^{-3} pc; Wang et al. 2001) puts the pulsar at a distance of 2.7 ± 0.35 kpc.

In the X-rays, PSR J1048−5832 was observed with the *Röntgen* Satellite (ROSAT) at 0.1–2.4 keV (Becker & Trümper 1997) and, soon after, with the Advanced Satellite for Cosmology and Astrophysics (ASCA) by Pivovaroff et al. (2000), who found possible evidence of extended X-ray emission associated with a PWN. More recent observations with *Chandra* (Gonzalez et al. 2006) confirmed the existence of the PWN, although they failed to detect pulsed X-ray emission, with a conservative 3σ upper limit of 53% on the pulsed fraction (0.5–10.0 keV). In γ-rays, PSR J1048−5832 was associated with the source 3EG J1048−5048 (Kaspi et al. 2000), detected by the EGRET instrument aboard CGRO, both on the basis of a spatial coincidence with the γ-ray source error box and of the tentative detection of γ-ray pulsations. Recently, these have been clearly detected at ≥0.1 GeV by *Fermi* (Abdo et al. 2009), with a double-peaked light curve.

Here, we report on the results of an archival VLT survey for *Fermi* pulsars. This paper is organised as follows: observations, data reduction, and analysis are described in Sect. 2, while results are presented and discussed in Sects. 3 and 4, respectively. Conclusions follow.

2. Observations and data reduction

2.1. Observation description

Optical images of the PSR J1357−6429 and PSR J1048−5832 fields were obtained with the VLT Antu telescope at the ESO Paranal observatory between April 2009 and February 2010 (see Table 1 for a summary of the observations) and are available in the public ESO archive[1]. Observations were performed in service mode with the FOcal Reducer/low dispersion Spectrograph (FORS2; Appenzeller et al. 1998), a multi-mode camera for imaging and long-slit/multi-object spectroscopy (MOS). FORS2 was equipped with its red-sensitive MIT detector, a mosaic of two 2 k × 4 k CCDs optimised for wavelengths longer than 6000 Å. In its standard resolution mode, the detector has a pixel size of 0.″25 (2 × 2 binning), which corresponds to a projected field-of-view of 8.′3 × 8.′3 over the CCD mosaic. However, due to vignetting, the effective sky coverage of the two detectors is smaller than the projected detector field-of-view and it is larger for the upper CCD chip. Observations were performed with the standard low gain, fast read-out mode and in high-resolution mode (0.″125/pixel) for PSR J1357−6429 and in standard resolution mode (0.″25/pixel) for PSR J1048−5832. In both cases, the target was positioned in the upper CCD chip. For PSR J1357−6429, bright stars close to the pulsar position were masked using the FORS2 MOS slitlets as occulting bars. Different filters were used: $v_{\rm HIGH}$ ($\lambda = 5570$ Å; $\Delta\lambda = 1235$ Å), $R_{\rm SPEC}$ ($\lambda = 6550$ Å; $\Delta\lambda = 1650$ Å), and $I_{\rm BESS}$ ($\lambda = 7680$ Å; $\Delta\lambda = 1380$ Å). To allow for cosmic ray removal and to minimise saturation of bright stars in the field, sequences of short exposures (from 200 to 750 s) were obtained per each target and per each filter. The total integration time was 14 700 s ($v_{\rm HIGH}$), 8800 s ($R_{\rm SPEC}$), and 1600 s ($I_{\rm BESS}$) for PSR J1357−6429 and of 24 000 s ($v_{\rm HIGH}$) for PSR J1048−5832. Exposures were taken in dark time and under photometric conditions[2], with an airmass mostly below 1.3 and sub-arcsecond image quality, as measured directly on the images by fitting the full-width at half maximum (FWHM) of unsaturated field stars.

2.2. Data reduction and astrometry

We reduced the data through standard packages in IRAF for bias subtraction and for flat-field correction using the closest-in-time bias and twilight flat-fields frames available in the ESO archive. For each band, we aligned and average-stacked the reduced science images using the IRAF task `drizzle` by applying a 3σ filter on the single pixel average to filter out residual hot and cold pixels and cosmic ray hits. Since all exposures were taken with sub-arcsec image quality, we did not make any selection prior to the image stacking. We applied the photometric calibration by using the extinction-corrected night zero points computed by the FORS2 pipeline and available through the instrument data-quality control database[3]. To register the pulsar positions on the FORS2 frames as precisely as possible, we recomputed their astrometric solution, which is, by default, based on the coordinates of the guide star used for the telescope pointing. Since most stars from the Guide Star Catalogue 2 (GSC-2; Lasker et al. 2008) are saturated in the stacked images, we used shorter exposures (10–15 s) of the fields taken with the same instrument configurations as those in Table 1 and available in the VLT archive. We measured the star centroids through Gaussian fitting using

[1] www.eso.org/archive
[2] http://archive.eso.org/asm/ambient-server
[3] www.eso.org/qc

Table 1. Summary of the available pulsar observations.

Pulsar	Date yyyy-mm-dd	Filter	T (s)	N	sec(z)	IQ ($''$)
PSR J1357−6429	2009-04-04	$v_{\rm HIGH}$	580	5	1.35	0.62 (0.03)
	2009-04-04	$R_{\rm SPEC}$	580	5	1.44	0.58 (0.03)
	2009-04-22	$v_{\rm HIGH}$	590	20	1.35	0.65 (0.03)
	2009-04-24	$R_{\rm SPEC}$	590	10	1.35	0.59 (0.04)
	2009-04-25	$I_{\rm BESS}$	200	8	1.31	0.57 (0.04)
PSR J1048−5832	2010-01-11	$v_{\rm HIGH}$	750	4	1.21	0.69 (0.04)
	2010-01-13	$v_{\rm HIGH}$	750	8	1.23	0.56 (0.03)
	2010-01-23	$v_{\rm HIGH}$	750	4	1.21	0.79 (0.04)
	2010-01-24	$v_{\rm HIGH}$	750	8	1.21	0.60 (0.03)
	2010-02-10	$v_{\rm HIGH}$	750	8	1.22	0.65 (0.03)

Notes. Reported are: the exposure times in s (T), the number of exposures (N), the average airmass sec(z) during the sequence of N exposures, the associated average image quality (IQ), and its rms (in parentheses).

the Graphical Astronomy and Image Analysis (GAIA) tool[4] and used the code ASTROM[5] to compute the pixel-to-sky coordinate transformation through a high-order polynomial, which accounts for the CCD distortions. For both pulsar fields, the rms of the astrometric fits was $\sigma_{\rm r} \sim 0\farcs1$ in the radial direction. To this value we added in quadrature the uncertainty $\sigma_{\rm tr} = 0\farcs1$ of the registration of the FORS2 image on the GSC2 reference frames, $\sigma_{\rm tr} = \sqrt{(3/N_{\rm s})}\sigma_{\rm GSC2}$, where $\sigma_{\rm GSC2} = 0\farcs3$ is the mean positional error of the GSC2 coordinates and $N_{\rm s}$ the number of stars used to compute the astrometric solution (Lattanzi et al. 1997). After accounting for the $\sim$0$\farcs$15 accuracy of the link of the GSC2 coordinates to the International Celestial Reference Frame (ICRF), we thus estimate that the overall (1σ) uncertainty of our FORS2 astrometry is $\delta_r \sim 0\farcs2$.

2.3. The problem of position: radio vs. X-rays

As a reference for our astrometry, we started from the most recently published radio positions of the two pulsars. Moreover, they both have precise X-ray positions obtained with *Chandra*. The published radio and X-ray coordinates of PSR J1357−6429 and PSR J1048−5832 are summarised in Table 2.

We note that the *Chandra* position of PSR J1357−6429 (Zavlin 2007) is quite different from what has been derived from the radio-interferometry observations performed with the Australia Telescope Compact Array (ATCA) by Camilo et al. (2004). Since this apparent inconsistency hampers the correct pulsar localisation on the FORS2 images, hence the search for its optical counterpart, we independently checked all the available sets of coordinates. Multiple *Chandra* observations are available for PSR J1357−6429, and we could use them to check the internal consistency of the *Chandra* astrometry. Firstly, we recomputed the X-ray position from the analysis of the two independent *Chandra*/HRC observations (Esposito et al. 2007; Zavlin 2007), and we found values consistent with the ones published in Zavlin (2007).

The pulsar has been recently observed also with the ACIS instrument (OBS-ID = 10880; MJD = 55 112.28). We downloaded the data from the public *Chandra* archive and found that the pulsar coordinates are also consistent, within the nominal *Chandra* position uncertainty of 0$\farcs$6[6] (90% confidence level), with those obtained with the HRC. We then averaged the three sets of coordinates, which yields $\alpha = 13^{\rm h}57^{\rm m}02\fs60$ and $\delta = -64°29'29\farcs80$ with a radial error of $\sim$0$\farcs$38. This implies a difference of $1\farcs23 \pm 0\farcs4$ between the *Chandra* and radio-interferometry positions.

Then, we verified the *Chandra* absolute astrometry by matching the positions of serendipitous X-ray sources detected in the *Chandra*/ACIS image with those of their putative counterparts detected in the 2MASS catalogue (Skrutskie et al. 2006). Since the accuracy of the *Chandra* astrometry rapidly degrades at large off-axis angles, we restricted our search to within 4′ of the centre of the ACIS field-of-view. In particular, we found 2MASS matches for four X-ray sources in the PSR J1357−6429 field. Although the uncertainty on the computed bore-sight correction does not yield any significant improvement in the absolute *Chandra* astrometry, the source match does not show any possible offsets between the optical and X-ray reference frames (both tied to the ICRF). Thus, we conclude that the *Chandra* coordinates are not affected by systematics. Similarly, we verified the published radio-interferometry position of PSR J1357−6429 against the radio-timing position obtained through more recent observations performed by the *Fermi* Pulsar Timing Consortium (Smith et al. 2008) and found that they are consistent, although the latter is probably affected by the pulsar timing noise and has much greater uncertainty.

In principle, the observed difference between the *Chandra* and the radio-interferometry positions of PSR J1357−6429 can be, at least partially, due to its still unknown proper motion. The time span between the epochs of the *Chandra* and the ATCA observations is ~7.17 yrs. This would imply a proper motion $\mu = 0\farcs17 \pm 0\farcs055$ yr^{-1} along a position angle $\theta = 70° \pm 15°$. We note that the *Chandra* observations of PSR J1357−6429 are distributed over a time span of ~3.9 yrs. Then, for the assumed single-epoch *Chandra* radial position uncertainty of 0$\farcs$6, they would only be sensitive to a proper motion of $\gtrsim$0$\farcs$55 yr^{-1} (3σ), i.e. larger than inferred from the comparison between the average *Chandra* position and the radio one. At the DM distance of ~2.4 kpc, the inferred proper motion would imply a transverse velocity of 2100 ± 700 km s^{-1}. This value is high, but after accounting for the associated uncertainty, it is not unheard of for a neutron star, as shown by the Guitar Nebula pulsar PSR B2224+65, whose transverse velocity could be as high as 1600 km s^{-1} (e.g., Chatterjee & Cordes 2004). Thus, the computed difference between the *Chandra* and radio positions of PSR J1357−6429 might, indeed, result in its first proper motion measurement. A similar case is that of the pulsar PSR J0108−1431, for which the comparison between its

[4] See star-www.dur.ac.uk/~pdraper/gaia/gaia.html
[5] www.starlink.rl.ac.uk/star/docs/sun5.htx/sun5.html
[6] http://asc.harvard.edu/cal/ASPECT/celmon

Table 2. Summary of the PSR J1357−6429 and PSR J1048−5832 coordinates (top and lower half, respectively) available from the literature from *Chandra* and radio timing (T) or interferometric (I) observations and the associated radial errors δr at the reference epoch (fourth column).

$\alpha^{(\mathrm{hms})}_{\mathrm{J2000}}$	$\delta^{(^\circ\,'\,'')}_{\mathrm{J2000}}$	$\delta\, r^{('')}$	MJD	Source
13 57 02.42	–64 29 30.20	0.15	51 785	Radio,I (1)
13 57 02.54	–64 29 30.00	0.60	53 693	*Chandra* (2)
13 57 02.60	–64 29 29.80	0.38	54 402	*Chandra* (3)
10 48 12.20	–58 32 05.80	1.21	50 889	Radio,T (4)
10 48 12.604	–58 32 03.75	0.08	50 581	Radio,I (5)
10 48 12.64	–58 32 03.60	0.55	52 859	*Chandra* (6)

References. (1) Camilo et al. (2004); (2) Zavlin (2007); (3) this work; (4) Wang et al. (2000); (5) Stappers et al. (1999); (6) Gonzalez et al. (2006).

Chandra and ATCA radio-interferometry positions also yielded first proof of a 3σ proper motion (Pavlov et al. 2009), confirmed by VLBI observations soon after (Deller et al. 2009). As in that case, future radio-interferometry observations will be crucial for confirming our tentative proper motion measurement of PSR J1357−6429.

For PSR J1048−5832, the *Chandra* position is also quite different ($4\farcs1 \pm 1\farcs3$) from the radio-timing one (Wang et al. 2000), obtained from observations performed with the Australia Telescope National Facility (ATNF) Parkes radio telescope. On the other hand, the difference with respect to the radio-interferometry position obtained from observations performed with the ATCA (Stappers et al. 1999) is not significant. As above, we verified all the available sets of coordinates. Firstly, we recomputed the X-ray position from the analysis of the *Chandra*/ACIS observation and found a value that is perfectly consistent with that published in Gonzalez et al. (2006). Then, we verified the *Chandra* absolute astrometry by matching the positions of 13 serendipitous X-ray sources detected in the *Chandra*/ACIS image with those of their putative 2MASS counterparts and found no evidence of possible offsets between the optical and X-ray reference frames. This implies that also the *Chandra* coordinates of PSR J1048−5832 are free from systematics. We also compared the Wang et al. (2000) radio-timing position with that obtained by the *Fermi* Pulsar Timing Consortium and found no obvious difference. The time span between the epochs of the *Chandra* and the radio-timing observations of PSR J1048−5832 is ∼5.39 yrs, which would imply a proper motion of $0\farcs76 \pm 0\farcs24$ yr^{-1}. At the DM distance of ∼2.7 kpc, this corresponds to a transverse velocity of 10250 ± 3250 km s^{-1}, which is much higher than the most extreme values derived from the known radio pulsar velocity distribution (e.g., Hobbs et al. 2005). Thus, the apparent inconsistency between the *Chandra* and radio-timing positions cannot be explained by the pulsar proper motion, but by a genuine difference in the astrometry of either of the two observations. In this respect, we note that the radio-timing position of Wang et al. (2000) is also inconsistent with the radio-interferometry one of Stappers et al. (1999), which suggests that the former might be affected by systematics and has to be taken with caution. Indeed, such an inconsistency has also been noted by Wang et al. (2000) who attributed it to the effect of timing noise following period irregularities after a glitch. We note that if we assume the radio-interferometry position of PSR J1048−5832 as a first-epoch reference, the more recent *Chandra* position would imply a proper motion $\mu \lesssim 0\farcs138$ yr^{-1} (1σ) along an unconstrained position angle.

Although the origin of the inconsistency between the *Chandra* and radio positions of the two pulsars is still debatable, and addressing it fully is beyond the goals of this work, we tend to favour the former and more recent ones. Thus, in the following we assume them as a reference. However, not to overlook any potential candidate counterpart, we also prudently evaluate any object detected in the VLT images at, or close to, the radio positions of the two pulsars.

3. Data analysis and results

The computed positions of PSR J1357−6429 and PSR J1048−5832 are shown in Fig. 1, overlaid on the stacked V-band FORS2 images of the two pulsars. The overall uncertainties on the pulsar positions account for the absolute error on the reference *Chandra* and radio coordinates (Table 2) and the accuracy of our astrometry recalibration of the FORS2 images ($0\farcs2$). However, to conservatively account for the unknown pulsar proper motions, in the following we extended our search radius up to three times the estimated 1σ uncertainties.

3.1. PSR J1357−6429

The radio position of PSR J1357−6429 (Fig. 1, left panel) falls ∼$0\farcs65$ from that of a relatively bright field star (Star A; $V = 21.8 \pm 0.06$), i.e at an angular distance equal to the ∼2–3σ radio position uncertainty. To quantitatively assess the significance of the association, we estimated the chance coincidence probability that an unrelated field object falls within a radius of $0\farcs65$ of the computed pulsar radio position. This probability can be computed as $P = 1 - \exp(-\pi\sigma r^2)$, where μ is the measured object density in the FORS2 upper CCD field-of-view (accounting for areas affected by vignetting and the areas masked by the occultation bars, see Sect. 2.1) and r is the matching radius ($0\farcs65$). The density of star-like objects (ellipticity $e < 0.2$) with magnitude $V \gtrsim 22$ in the field-of-view is $\mu \sim 0.005$/sq. arcsec. This yields an estimated chance coincidence probability $P \sim 9\times10^{-3}$, which is not statistically compelling yet.

To qualitatively verify the reliability of such an association, we compared the brightness of Star A with what is expected from the pulsar. PSR J1357−6429 has a rotational energy loss $\dot{E} \sim 3.1 \times 10^{36}$ erg s^{-1}. If we assume an efficiency in converting spin-down power into optical luminosity $\eta_{\mathrm{opt}} \equiv L_{\mathrm{opt}}/\dot{E}$ comparable to that of, e.g. the ∼11 kyr old Vela pulsar, we would expect an optical luminosity for PSR J1357−6429 that is lower by only a factor of ∼2, after scaling for the Vela rotational energy loss ($\dot{E} \sim 6.9 \times 10^{36}$ erg s^{-1}). At the PSR J1357−6429 distance (2.4 ± 0.6 kpc) and for the corresponding interstellar extinction ($A_V = 2.2^{+1.7}_{-1.1}$), computed from the $N_{\mathrm{H}} = 0.4^{+0.3}_{-0.2} \times 10^{22}$ cm^{-2} obtained from the spectral fits to the *XMM-Newton* spectrum (Esposito et al. 2007) using the relation of Predhel & Schmitt (1995) and the extinction coefficients of Fitzpatrick (1999), we then derive an expected magnitude in the range $V \sim 29.5$–33.4, accounting for both the distance and interstellar extinction uncertainties. Obviously, these values are not within reach for any current 10 m-class telescope. On the other hand, if PSR J1357−6429 had an efficiency comparable to that of the younger ($\tau \sim 1$ kyr) and more energetic ($\dot{E} \sim 4.6 \times 10^{38}$ erg s^{-1}) Crab pulsar, the same scaling as above would yield an expected magnitude of $V \sim 21.1$–24.9. Thus, if Star A were the pulsar's optical counterpart, PSR J1357−6429 would have an emission efficiency either comparable to or up to ∼15 times higher than

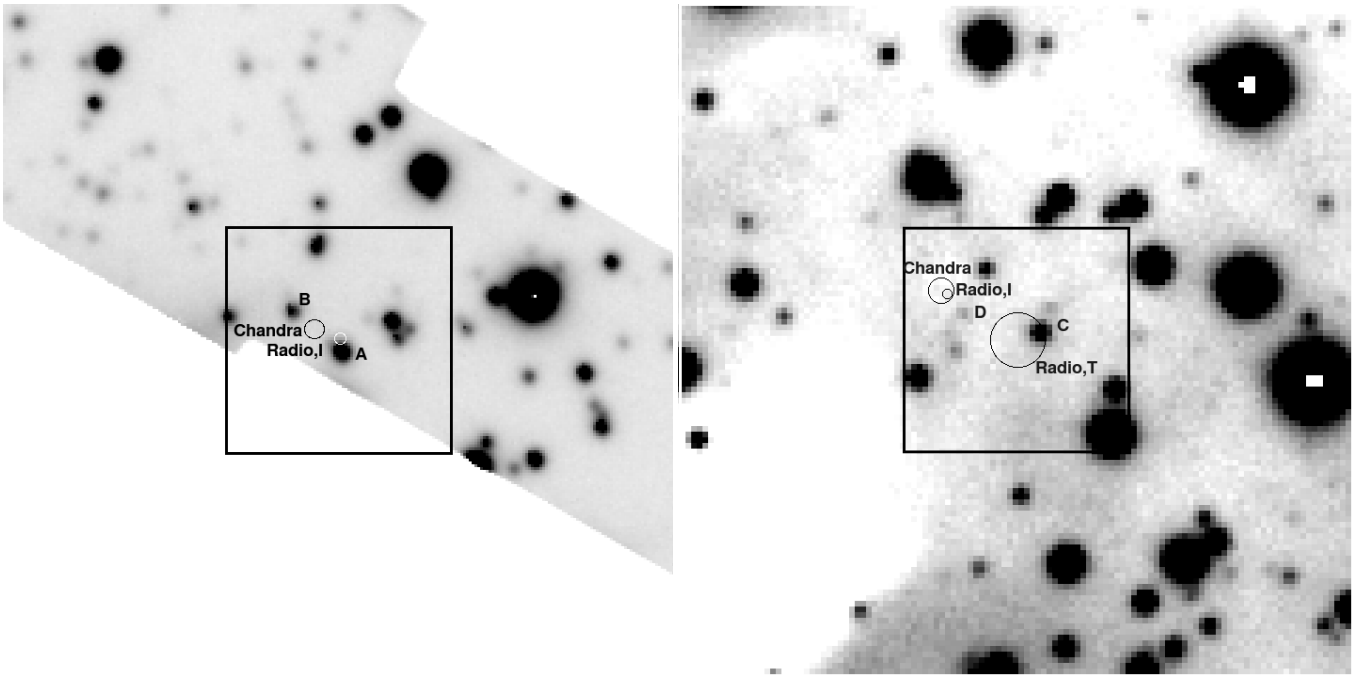

Fig. 1. VLT/FORS2 observations of PSR J1357−6429 (*left*) and PSR J1048−5832 (*right*) taken in the $v_{\rm HIGH}$ filter, with integration times of 14 700 and 24 000 s, respectively. North is at the top, east to the left. Image cutouts are 30″×30″ in size. The circles marks the pulsar radio (T = timing; I = interferometric) and *Chandra* positions derived according to our astrometry re-calibration (Sect. 2.2). Their radius account for the absolute error on the reference X-ray/radio coordinates (Table 2) and the accuracy of our optical astrometry (0.″2). The radii of the error circles are ∼0.″43 and ∼0.″25 for the *Chandra* and radio-interferometry coordinates of PSR J1357−6429, respectively, and ∼0.″58, ∼0.″22, and ∼1.″22, for the *Chandra*, radio-interferometry, and radio-timing coordinates of PSR J1048−5832, respectively. The white areas in the left panel correspond to the edges of the occulting bars used in the FORS2 frame to mask bright stars close to the pulsar position. The clumpy white structure in the right panel is part of an extended nebulosity detected in the PSR J1048−5832 field (see Sect. 3.2). In both panels, the square (10″ × 10″) corresponds to the area shown in Fig. 3.

the Crab. Thus, the association would be possible, in principle, at least based on the pulsar's energetics and on an assumed Crab-like optical emission efficiency. However, we note that pulsar optical emission efficiencies have been computed for less than ten objects, and their dependance on the pulsar parameters, such as their spin-down age, is still unclear. Therefore, we followed an independent approach to estimating the expected pulsar's brightness using as reference the relation between the non-thermal X-ray and optical luminosities measured for pulsars with identified X-ray/optical counterparts (e.g., Zharikov et al. 2004, 2006). In this case, taking the rather large uncertainty affecting this relation into account, as well as the uncertainty on the X-ray spectral parameters of PSR J1357−6429 (Esposito et al. 2007), hence on the non-thermal X-ray luminosity, we end up with an expected magnitude in the range of $V \sim 26.2$–31.2, i.e. much fainter than for star A. As a further test, we also compared the colours of Star A ($V = 21.80 \pm 0.06$; $R = 20.65 \pm 0.03$; $I = 19.75 \pm 0.03$) with those of field stars, as measured on the short exposures to (i) avoid both problems in background subtraction for stars close to the occulting bars and saturation problems and to (ii) homogeneously cover the unmasked FORS2 field-of-view. The two V-$(V - R)$ and V-$(V - I)$ colour–magnitude diagrams (CMDs) are shown in Fig. 2. As seen, the location of Star A in both CMDs is along the sequence of field stars, implying that it has no peculiar colours and that its association with the pulsar is unlikely. For instance, for a flat power-law spectrum $F_\nu \propto \nu^{-\alpha}$, like that of e.g. the Vela pulsar (Mignani et al. 2007), we would expect $(V - R) \approx 0.2$ and $(V - I) \approx 0.1$, after accounting for the interstellar extinction towards PSR J1357−6429, which are obviously off the main sequence in both CMDs. Thus, on the basis of the comparison with the optical emission efficiency of pulsars with known optical counterparts, their relative X-ray-to-optical brightness, and the colours of Star A, we consider it unlikely that it is the pulsar's counterpart.

We then searched for possible counterparts at our revised *Chandra* position. We note that this overlaps with an apparent enhancement over the sky background noticed in the co-added I-band image (Fig. 3, left). However, it is difficult to determine whether such an enhancement comes from a background fluctuation, perhaps produced by the superposition of the PSF wings of the two adjacent stars detected southwest (Star A) and northeast (Star B) of the *Chandra* position and of the bright masked star southeast of them, or if it is associated with a real source. Unfortunately, the difficulties in the PSF subtraction of the two stars, with Star A possible blended with a fainter star and Star B at the edge of occulting bar and partially blended with a bright star, do not allow us to better resolve the background enhancement. If associated with a point source, it would correspond to a magnitude $I \approx 24.6$. Interestingly enough, such an enhancement is only recognisable in the I-band image and not in the longer integration R and V-band ones. This would suggest that either it is not associated with a real object or, if it is, that the object's spectrum is either quite red and/or affected by an interstellar extinction probably greater than measured in the pulsar's direction. To verify there is an object at the *Chandra* position, we inspected the single I-band images. However, their short integration time (200 s) makes it difficult to recognise any obvious systematic flux enhancement at the expected location. We also smoothed the images using a Gaussian filter over 3 × 3 pixel cells, but this did not yield any clearer detection. Thus, it is difficult to prove that the background enhancement seen at the pulsar *Chandra* position in the I-band image is unambiguously

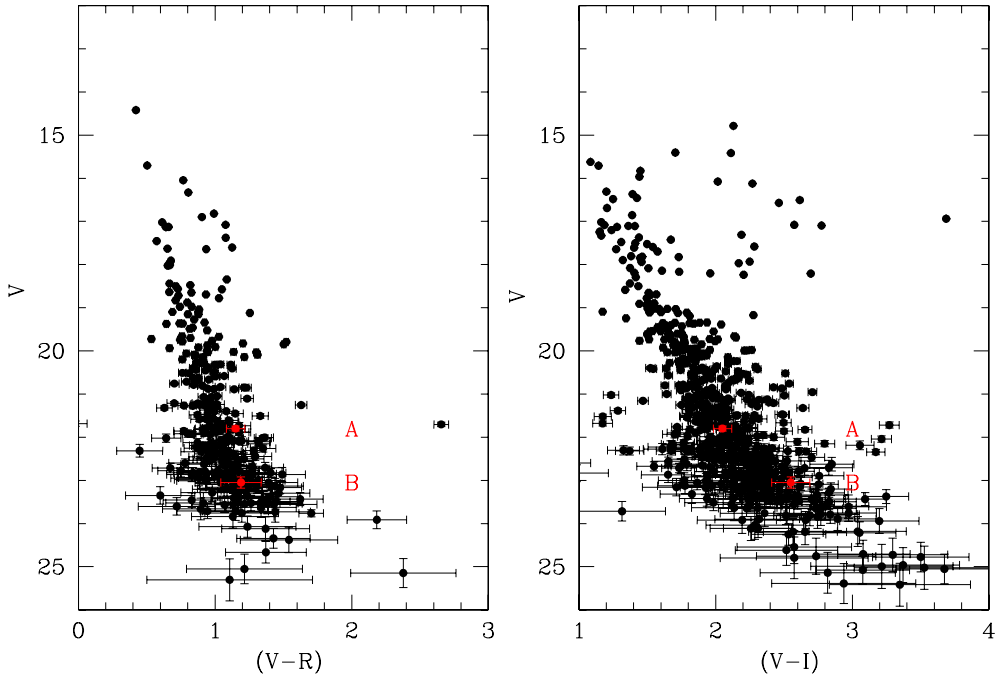

Fig. 2. Observed (not extinction-corrected) colour-magnitude diagrams of all the objects detected in the PSR J1357−6429 field. The two objects detected closest to the radio (Star A) and *Chandra* (Star B) pulsar positions (Fig. 1) are marked in red, with magnitudes $V = 21.8 \pm 0.06$ and $V = 23.05 \pm 0.13$, respectively. The photometry errors are purely statistical and do not account for the systematic uncertainties on the absolute flux calibrations.

associated with a real object. Higher spatial resolution observations with the HST would be crucial for resolving this putative object against the noisy background produced by the PSF of Stars A and B and confirm it as a candidate optical counterpart to PSR J1357−6429.

No other possible counterpart is detected within the computed pulsar *Chandra* error circle (Fig. 3, left). Star B is at ∼1.″4, i.e. $\approx 3\sigma$ from the best-estimate *Chandra* position. Moreover, both its fluxes ($V = 23.05 \pm 0.13$; $R = 21.86 \pm 0.07$; $I = 20.5 \pm 0.05$) and colours (Fig. 2) are comparable to those of Star A, already ruled out as a candidate counterpart (see above). Thus, assuming that PSR J1357−6429 is not detected in the FORS2 images, we computed the pulsar flux upper limits in the *VRI* bands. Following a standard approach (e.g., Newberry 1991), we determined the number of counts corresponding to a 3σ detection limit in a photometry aperture of 1″ diameter (8 pixels) from the standard deviation of the background sampled within the *Chandra* error circle. After applying the aperture correction, computed from the measured PSF of a number of relatively bright but unsaturated stars in the field, we then derived 3σ upper limits of $V \sim 27$ and $R \sim 26.8$ at the *Chandra* position, while in the *I* band we conservatively assumed a flux of $I \approx 24.6$ measured above as our upper limit estimate.

3.2. PSR J1048−5832

The field of PSR J1048−5832 shows large extended structures where both the sky brightness and the star density are much lower then in the rest of the field. These structures are present in the single FORS2 raw frames taken days apart so that they are not an artefact due to, e.g. an incorrect flat fielding or to the unreported presence of clouds at the moment of the observations. We did check the *R*-band images of the Digitised Sky Survey (DSS) and found that the same structures are visible with the same extent and position as seen in the FORS2 images, which proves that they are real and not caused by any instrumental or atmospheric effects. We used the DSS to look for such structures on scales as large as $40' \times 40'$ and found that they apparently connected to other similar structures extending on a sort of regular pattern. We also checked the 2MASS *JHK*-band images that, instead, show evidence of neither such structures nor of under-density of stars at their expected locations. Thus, we conclude that they are most likely dense molecular clouds along the plane of the Milky Way, possibly part of the CH_3OH maser associations in nearby star-forming regions (e.g. Goedhart et al. 2004).

Although no counterpart to PSR J1048−5832 has been yet proposed in the literature, we note that an observing programme[7] has been recently carried out at the VLT to follow up on the claimed detection of a candidate counterpart, presumably in the same data set used in this work. This prompted us to prudently screen each object detected close to the published positions of PSR J1048−5832. In particular, we note that its radio-timing position (Fig. 1, right panel) falls close to a $V \sim 24$ object (Star C), even detected in the short 15 s exposures used for the image astrometry, right on the edge of the radio error circle (∼1.″22). Again, based on position alone, we cannot rule out that Star C is associated with the pulsar. However, the probability of a chance coincidence with field objects of magnitude $V \gtrsim 24$ is $P \sim 0.04$, i.e. certainly not low enough to statistically claim an association. In addition, such an association is problematic from the point of view of the pulsar's energetics. As in Sect. 3.1, we compared the brightness of Star C with what is expected for the pulsar. By assuming an optical efficiency comparable to that of the Vela pulsar, PSR J1048−5832's rotational

[7] *Confirming the detection of a Fermi gamma-ray pulsar in the optical*, PI Sollerman, 386.D-0585(A).

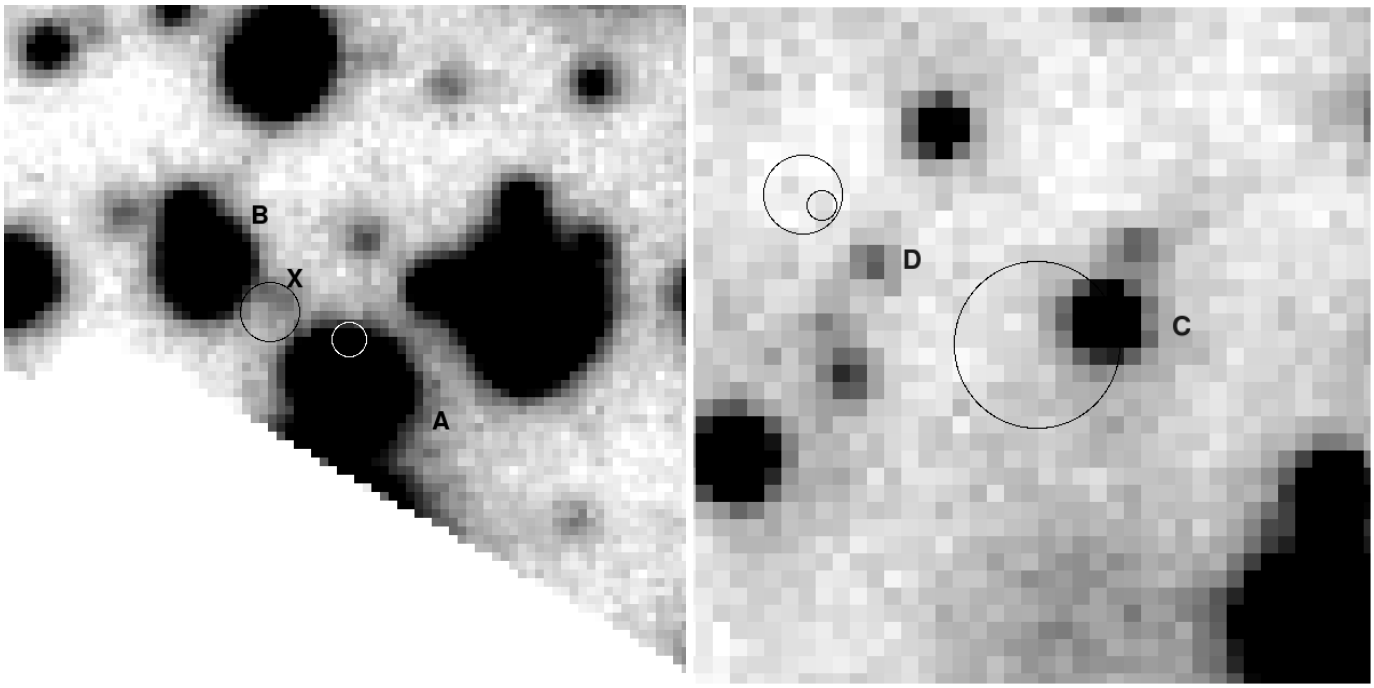

Fig. 3. 10″ × 10″ zooms of the PSR J1357−6429 (*left*) and PSR J1048−5832 images (*right*) taken through the $I_{\rm BESS}$ (1800 s) and the $v_{\rm HIGH}$ filter (24 000 s), respectively. In both cases, the colour scale has been stretched to highlight fainter objects. A flux enhancement (labelled with X) is seen at the *Chandra* position of PSR J1357−6429, which might be due either to a background fluctuation or to an unresolved object in the PSF of the two adjacent stars A and B (see text for discussion).

energy loss ($\dot{E} \sim 2 \times 10^{36}$ erg s^{-1}) would then imply only a factor of ∼ 3 lower optical luminosity. Following the same analysis as for PSR J1357−6429 (see Sect. 3.1), at the PSR J1048−5832 distance (2.7 ± 0.35 kpc) and for the corresponding interstellar extinction ($A_V = 5^{+2.2}_{-1.1}$), derived from the $N_H = 0.9^{+0.4}_{-0.2} \times 10^{22}$ cm^{-2} (Marelli et al. 2011), we determine an expected magnitude $V \sim 33.3$–37, accounting for both the distance and interstellar extinction uncertainties. Similarly, assuming more optimistically an emission efficiency comparable to that of the Crab pulsar, we derived an expected magnitude of $V \sim 25$–28.7. This means that, if Star C were indeed the PSR J1048−5832 optical counterpart, the pulsar should have an emission efficiency ∼2–80 times higher than the Crab. On the other hand, by using the relation between the X-ray and optical luminosity (Zharikov et al. 2004, 2006) as in Sect. 3.1, we obtain a magnitude in the range $V \sim 29$–34. Thus, Star C cannot be the pulsar optical counterpart.

Then, we searched for a possible counterpart at the pulsar *Chandra* position. No object is detected within, or close to, the *Chandra* (0.″55) error circle apart from a faint object (Star D; $V \sim 26.7$) visible ∼1.″6 southwest of it (Fig. 3, right). However, the offset is about three times the 1σ uncertainty on the pulsar position. Thus, we deem the association unlikely both on the basis of the loose positional coincidence and on statistical grounds, with a chance coincidence probability of $P \sim 0.08$. Moreover, the lack of colour information makes it impossible to constrain the nature of this object. Therefore, we conclude that PSR J1048−5832 is not detected in the FORS2 image. Following the same procedure as in Sect. 3.1, we determined the number of counts corresponding to a 3σ detection limit in a 1″ photometry aperture (4 pixel) from the standard deviation of the background sampled within the *Chandra* error circle. After applying the aperture correction, this yields a 3σ detection limit of $V \sim 27.6$.

3.3. Search for the optical PWNe

To verify the possible presence of PWNe in the optical, we have over-plotted the X-ray contours of the *Chandra*/ACIS images of PSR J1357−6429 and PSR J1048−5832 on the FORS2 V-band images (Fig. 4). The X-ray PWNe of PSR J1357−6429 has been discovered in a recent ∼59 ks *Chandra*/ACIS image (Lemoine-Goumard et al. 2011; Chang et al. 2011) and has a much greater angular extent than the compact PWN ($\lesssim$ 4″) tentatively detected by Zavlin (2007) in an older ∼33 ks *Chandra*/HRC data set. We note that the proximity of the PSR J1357−6429 position to the FORS2 occulting bars and the relative crowding of the field makes it very difficult to search for the optical counterpart of its X-ray PWN. In particular, the bright core of the PWN overlaps with the position of Stars A and B, and it is partially masked by the occulting bars south of it. Due to the relatively high fluxes of Stars A and B with respect to what is expected for a putative optical PWN, the uncertainty in the PSF subtraction residuals makes its detection improbable. At the same time, the faint PWN tail overlaps with several stars detected northeast of the pulsar's *Chandra* position (Fig. 4, left). Thus, any upper limit on the optical surface brightness of the PWN would be highly uncertain and hampered by the partially covered area. We note that a PWN around PSR J1357−6429 has been detected at TeV energies by HESS (Abramowski et al. 2001), but its angular size is much larger than the entire FORS2 field-of-view, by itself masked by ∼50% by the occulting bars. In the case of PSR J1048−5832, the proximity of the *Chandra* position to one of the clumps belonging to the large molecular cloud complex detected in the field (Fig. 4, right) makes it difficult to search for optical emission along the whole PWN, whose angular extent (6″×11″; Gonzalez et al. 2006) is partially covered by the clump. In particular, the clump entirely covers the PWN tail, which extends southeast of the pulsar position. No extended optical emission is recognised close to the head of the PWN, where the clumps are sparser and

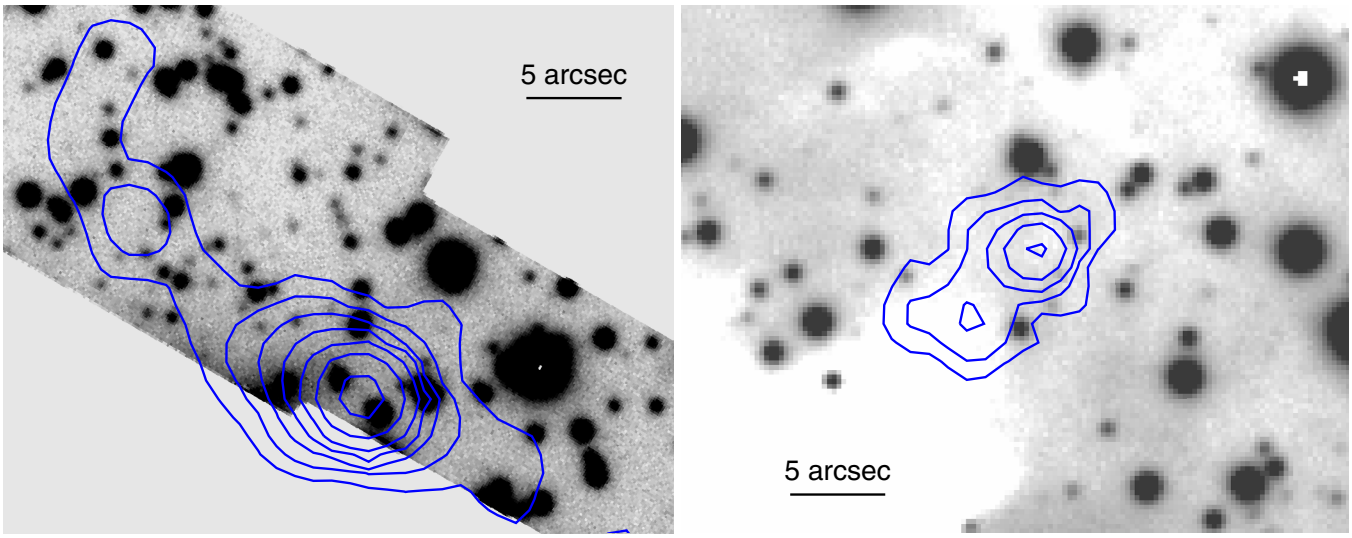

Fig. 4. Zooms of the PSR J1357−6429 (*left*) and PSR J1048−5832 (*right*) FORS2 *V*-band images. The blue contours correspond to the isophotes underlying the structure of the PWNe observed by *Chandra* in the 0.5–4 keV range. In both cases, a smoothing with a Gaussian kernel of 1″ has been applied. The contours have logarithmic spacing, with a factor of 2 step in surface brightness.

smaller. As in the case of PSR J1357−6429, any upper limit of the optical surface brightness of the PWN is hampered by the covered area.

4. Discussion

We compared our optical flux upper limits in the *V* band with the pulsars' rotational energy loss rates. For PSR J1357−6429, our upper limit of $V \sim 27$ corresponds to an optical luminosity upper limit $L_{\rm opt} \sim 0.6$–21.6×10^{29} erg s^{-1}, for a distance $d = 2.4 \pm 0.6$ kpc and for an interstellar extinction $A_V = 2.2^{+1.7}_{-1.1}$, after accounting for their associated uncertainties. This implies an emission efficiency upper limit $\eta_{\rm opt} \sim 0.2$–7×10^{-7}. This value is at least a factor of 5 lower than the Crab pulsar and, possibly, closer to that of the Vela pulsar. On the other hand, for PSR J1048−5832 our upper limit of $V \sim 27.6$ implies (for $d = 2.7 \pm 0.35$ kpc and $A_V = 5^{+2.2}_{-1.1}$) upper limits of $L_{\rm opt} \sim 0.4$–12.5×10^{30} erg s^{-1} and $\eta_{\rm opt} \sim 1.8$–62.5×10^{-7}. In principle, this does not rule out optical emission efficiency comparable to that of the Crab pulsar, although the pulsar spin-down age (20.3 kyr) might also suggest in this case, Vela-like emission efficiency. An optical emission efficiency $\eta_{\rm opt} \lesssim 10^{-7}$–$10^{-6}$ has been measured also from the upper limit on the optical emission of PSR B1706−44, the only other Vela-like pulsar for which VLT observations are available (e.g. Mignani et al. 1999). This would confirm that Vela-like pulsars are intrinsically less efficient emitters in the optical than Crab-like pulsars, possibly even less efficient than middle-aged and old pulsars, like PSR B0656+14, Geminga, PSR B1055−52, PSR B1929+10, and PSR B0950+08. The measurement of such a low emission efficiency in the optical band for Vela-like pulsars might then provide useful information on emission models of the neutron star magnetosphere.

We compared the flux upper limits of PSR J1357−6429 and PSR J1048−5832 with the extrapolations in the optical domain of the X and γ-ray spectra. For PSR J1357−6429, we assumed the X-ray spectral model of Esposito et al. (2007), a power law (PL) with photon index $\Gamma_{\rm X} = 1.4 \pm 0.5$ plus a blackbody (BB) with temperature $kT = 0.16^{+0.09}_{-0.04}$ keV ($N_{\rm H} = 0.4^{+0.3}_{-0.2} \times 10^{22}$ cm^{-2}), and the γ-ray spectral model of Lemoine-Goumard et al. (2011), a PL with photon index $\Gamma_\gamma = 1.54 \pm 0.41$, and exponential cut-off at ∼0.8 GeV. For PSR J1048−5832, we assumed the X-ray spectral model of Marelli et al. (2011), a PL with photon index $\Gamma_{\rm X} = 2.4 \pm 0.5$ ($N_{\rm H} = 0.9^{+0.4}_{-0.2} \times 10^{22}$ cm^{-2}), and the γ-ray spectral model of Abdo et al. (2009), a PL with photon index $\Gamma_\gamma = 1.38 \pm 0.13$ and exponential cut-off at ∼2.3 GeV. Our optical flux upper limits are corrected for interstellar extinction based upon the $N_{\rm H}$ derived from the fit to the X-ray spectra. The multi-wavelength spectral energy distributions (SEDs) of the two pulsars are shown in Fig. 5, where we accounted for both the 1σ uncertainty on the extrapolations of the X and γ-ray PL and the uncertainty on the extinction-corrected flux upper limits. For PSR J1357−6429 (Fig. 5, left) we see that the optical flux upper limits can be compatible with the extrapolation of the X-ray PL. Thus, it is possible that the expected optical PL spectrum indeed follows the extrapolation of the X-ray one, a case so far observed only for PSR B1509−58 among all the optically-identified pulsars (see, e.g. Mignani et al. 2010a). The optical flux upper limits are also compatible, with the possible exception of the R-band one, with the extrapolation of the γ-ray PL, which does not allow us to prove that there is a break in the optical/γ-ray spectrum, as observed in other pulsars. Indeed, a possible consistency between the γ-ray and optical PL spectra has been found so far for only a minority of cases (Mignani et al., in prep.), such as the middle-aged pulsar PSR B1055−52 (Mignani et al. 2010b). The multi-wavelength SED is different in the case of PSR J1048−5832 (Fig. 5, right), for which the optical *V*-band upper limit is compatible with the extrapolation of the steep X-ray PL only for the highest values of the $N_{\rm H}$, but is well above the extrapolation of the flat γ-ray one. This does not rule out there being a break in the optical/X-ray PL spectrum, as observed in most pulsars (Mignani et al. 2010a), and the optical spectrum following the extrapolation of the γ-ray PL. Interestingly enough, at variance with PSR J1357−6429, no single model can describe the optical-to-γ-ray magnetospheric emission of PSR J1048−5832.

Thus, the comparison between the multi-wavelength SEDs of these two Vela-like pulsars suggests that the occurrence of spectral breaks might not correlate with the pulsar's age. Of course, the uncertainty on the spectral parameters of PSR J1357−6429, especially in the γ-ray band, makes it difficult

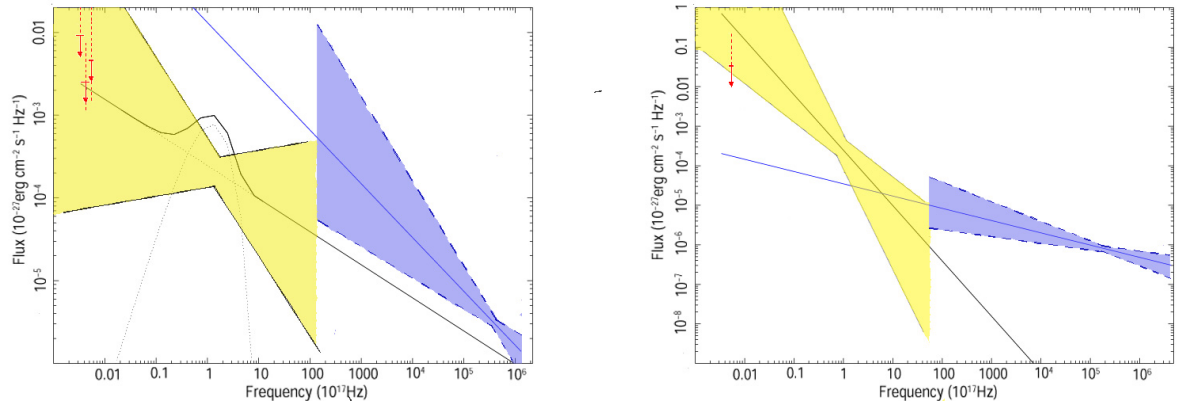

Fig. 5. Upper limits on the extinction-corrected optical fluxes of PSR J1357−6429 (*left*) and PSR J1048−5832 (*right*) compared with the low-energy extrapolations of the X-ray (solid black) and γ-ray (solid blue) spectral models that best fit the *XMM-Newton*, *Chandra* (Esposito et al. 2007; Marelli et al. 2011), and *Fermi* (Lemoine-Goumard et al. 2011; Abdo et al. 2009) data. The plotted optical flux upper limits are corrected for interstellar extinction based upon the best-fit value of the $N_{\rm H}$. The dotted lines in the left panel correspond to the PL and BB components to the model X-ray spectrum. In both panels, the yellow and blue-shaded areas (left to right) indicate the 1σ uncertainty on the extrapolations of the X and γ-ray PLs, respectively. The vertical red dashed lines mark the uncertainty on the extinction-corrected optical flux upper limits, computed around the best-fit value of the $N_{\rm H}$. For PSR J1357−6429, we neglected the uncertainties on the extrapolation of the BB component, whose contribution in the optical band is negligible.

to draw any conclusion. As new data are taken by *Fermi*, it will be possible to better constrain the value of the pulsar's γ-ray photon index and verify the possible absence of spectral breaks and its dissimilarity with PSR J1048−5832.

5. Summary and conclusions

We used archival VLT/FORS2 observations to perform the first deep optical investigations of the two *Fermi* pulsars PSR J1357−6429 and PSR J1048−5832. We re-assessed the positions of the two pulsars from the analyses of all the available *Chandra* observations and a comparison with the published radio positions. For PSR J1357−6429, this yielded a tentative proper motion of $\mu = 0\farcs17 \pm 0\farcs055$ yr^{-1} ($70° \pm 15°$ position angle), which needs to be confirmed by future radio-interferometry observations. For PSR J1048−5832, we concluded that its radio-timing position is either wrong or affected by large uncertainties caused by timing irregularities. For both pulsars, none of the objects detected around the *Chandra* positions can be considered viable candidate counterparts on the basis of their relatively large optical flux, $\gtrsim 3\sigma$ offset from the pulsar position, and lack of peculiar colours with respect to the field stars.

For PSR J1357−6429, we found a marginal evidence of a flux enhancement over the background at the edge of the *Chandra* error circle, which might come from the presence of a faint source ($I \approx 24.6$). However, the local crowding, with two relatively bright stars within a radius of $\sim 1\farcs5$ from the *Chandra* position, and the lack of detections in the V and R-bands, make it problematic to determine whether such an enhancement come from a background fluctuation, perhaps produced by the PSF wings of the two stars, or it is associated with a real source and hence to a putative pulsar counterpart. Assuming that PSR J1357−6429 is not detected in the VLT images, we determined 3σ upper limit on its optical brightness of $V \sim 27$. This implies an optical emission efficiency of $\eta_{\rm opt} \lesssim 7 \times 10^{-7}$, at least a factor of 5 lower than the Crab pulsar and, possibly, more compatible with that of the Vela pulsar. For PSR J1048−5832, our 3σ upper limit of $V \sim 27.6$ implies an optical emission efficiency $\eta_{\rm opt} \lesssim 6 \times 10^{-6}$, which is still compatible with a Crab-like optical emission efficiency. Finally, in both cases we did not find evidence for possible optical counterparts of the PWNe detected in X-rays by *Chandra*, with the search complicated by the field crowding and the partial occultation at the pulsar position for PSR J1357−6429, and by the presence of the molecular cloud complex for PSR J1048−5832.

The VLT observations presented here are close to the sensitivity limits achievable with 10m-class telescopes under sub-arcsec seeing conditions. In the case of PSR J1357−6429, deep, high spatial resolution images with the HST are probably required to firmly claim an object detection from the flux enhancement seen at the *Chandra* position. Moreover, if our tentative proper motion measurement is confirmed by future radio-interferometry observations, the pulsar will be close to occultation by the nearby Star B in mid 2012 and it will remain occulted for the next ten years. Thus, prompt HST follow-up observations in the I-band are the only way to achieve the optical identification of PSR J1357−6429. In the case of PSR J1048−5832, the large interstellar extinction ($A_V \sim 5$) and the presence of the molecular cloud complex in the field hamper observations in the optical/near-ultraviolet. Deep observations in the near-infrared, either with the HST or with adaptive optic device at 10m-class telescopes, might represent a better opportunity to spot a candidate counterpart to the pulsar.

Acknowledgements. The authors thank the *Fermi* Pulsar Timing Consortium, in particular David Smith, Ryan Shannon, and Simon Johnston, for checking for updated radio coordinates of the two pulsars. We also thank the *Fermi* Publication Board and the anonymous referee for their useful comments on the manuscript.

References

Abdo, A. A., Ackermann, M., Ajello, M., et al. 2009, ApJ, 706, 1331
Abdo, A. A., Ackermann, M., Ajello, M., et al. 2010, ApJS, 187, 460
Abdo, A. A., et al. 2011, ApJS, submitted [arXiv:1108.1435]
Abramowski, A., the H. E. S. S. Collaboration 2011, A&A, in press [arXiv:1108.2855]
Appenzeller, I., Fricke, K., Fürtig, W., et al. 1998, The Messenger, 94, 1
Atwood, W. B., Abdo, A. A., Ackermann, M., et al. 2009, ApJ, 697, 1071
Becker, W., & Trümper, J. 1997, A&A, 326, 682
Camilo, F., Manchester, R. N., Lyne, A. G., et al. 2004, ApJ, 611, L25

Chang, C., Pavlov, G. G., & Kargaltsev, O. 2011, ApJ, submitted [arXiv:1107.1819]
Chatterjee, S., & Cordes, J. M. 2004, ApJ, 600, L51
Cordes, J. M., & Lazio, T. J. W. 2002 [arXiv:astro-ph/0207156]
Deller, A. T., Tingay, S. J., Bailes, M., & Reynolds, J. E. 2009, ApJ, 701, 1243
Esposito, P., Tiengo, A., de Luca, A., & Mattana, F. 2007, A&A, 467, L45
Fitzpatrick, E. L. 1999, PASP, 111, 63
Goedhart, S., Gaylard, M. J., & Van der Walt, D. J. 2004, MNRAS, 355, 553
Gonzalez, M. E., Kaspi, V. M., Pivovaroff, M. J., & Gaensler, B. M. 2006, ApJ, 652, 569
Johnston, S., Lyne, A. G., Manchester, R. N., et al. 1992, MNRAS, 255, 401
Hobbs, G., Lorimer, D. R., Lyne, A. G., & Kramer, M. 2005, MNRAS, 360, 974
Kaspi, V. M., Lackey, J. R., Mattox, J., et al. 2000, ApJ, 528, 445
Lasker, B. M., Lattanzi, M. G., McLean, B. J., et al. 2008, AJ, 136, 735
Lattanzi, M. G., Capetti, A., & Macchetto, F. D. 1997, A&A, 318, 997
Lemoine-Goumard, M., Zavlin, V. E., Grondin, M-H., et al. 2011, A&A, 533, A102
Marelli, M., De Luca, A., & Caraveo, P. A. 2011, ApJ, 733, 82
Mignani, R. P. 2009a, in Neutron Stars and Gamma Ray Bursts, AIP, in press [arXiv:0908.1010]
Mignani, R. P. 2009b, The Messenger, 138, 19
Mignani, R. P. 2010a, in Astronomy with Megastructures, in press [arXiv:1008.5037]
Mignani, R. P. 2010b, in ASTROphysics of Neutron Stars 2010, in press [arXiv:1009.3378]
Mignani, R. P. 2010c, in The impact of HST on european astronomy, A&SpSci. Proc., 47
Mignani, R. P. 2011, AdSpR, 47,1281
Mignani, R. P., Caraveo, P. A., & Bignami, G. F. 1999, A&A, 343, L5
Mignani, R. P., Zharikov, S., & Caraveo, P. A. 2007, A&A, 473, 891
Mignani, R. P., Sartori, A., De Luca, A., et al. 2010a, A&A, 515, A110
Mignani, R. P., Pavlov, G. G., & Kargaltsev, O. 2010b, ApJ, 720, 1635
Mignani, R. P., Razzano, M., De Luca, A., et al. 2011, A&A, submitted
Monet, D. G., Levine, S. E., Canzian, B., et al. 2003, AJ, 125, 984
Newberry, M. V. 1991, PASP, 103, 122
Pavlov, G. G., Kargaltsev, O., Wong, J. A., & Garmire, G. P. 2009, ApJ, 691, 458
Predehl, P., & Schmitt, J. H. M. M. 1995, A&A, 293, 889
Shearer, A., & Golden, A. 2001, ApJ, 547, 967
Shearer, A., et al. 2010, in High Time Resolution Astrophysics IV, PoS [arXiv:1008.0605]
Skrutskie, M. F., Cutri, R. M., Stiening, et al. 2006, AJ, 131, 1163
Smith, D. A., Guillemot, L., Camilo, F., et al. 2008, A&A, 492, 923
Stappers, B. W., Gaensler, B. M., & Johnston, S. 1999, MNRAS, 308, 609
Thompson, D. J. 2008, Rep. Prog. Phys., 71, 226901
Wang, N., Manchester, R. N., Pace, R. T., et al. 2000, MNRAS, 317, 843
Weltevrede, P., Johnston, S., Manchester, R. N., et al. 2010, PASP, 27, 64
Zavlin, V. E. 2007, ApJ, 665, L143
Zharikov, S. V., Shibanov, Yu. A., Mennickent, R. E., et al. 2004, A&A, 417, 1017
Zharikov, S. V., Shibanov, Yu. A., & Komarova, V. N. 2006, AdSpR, 37, 1979